Flow-field and Noise Characterization of a Controlled-Diffusion Airfoil subject to flow separation and stall

Kalyani, S.K.; Moreau, Stéphane ; Ragni, D.

DOI
10.2514/6.2022-2894

Publication date
2022

Document Version
Final published version

Published in
28th AIAA/CEAS Aeroacoustics 2022 Conference

Aeroacoustics Conferences
June 14-17, 2022, Southampton, UK
28th AIAA/CEAS Aeroacoustics 2022 Conference

10.2514/6.2022-2894

Flow-field and Noise Characterization of a Controlled-Diffusion Airfoil subject to flow separation and stall

Sidharth Krishnan Kalyani*, Stéphane Moreau† and Daniele Ragni‡

The present experimental investigation in the anechoic wind tunnel of university of Sherbrooke focuses on the flow-field and noise characterization of a Controlled Diffusion (CD) airfoil, with the flow transitioning from an attached boundary layer at 15° incidence to a completely detached one (deep stall) at 22° incidence. Simultaneous unsteady wall-pressure and far-field measurements are performed to investigate the effect of Reynolds number on the separation and stalling noise signature of the CD airfoil. Spanwise coherence exhibits a bi-modal shape with levels of coherence shifting towards lower frequencies and increasing in value with increasing incidences. Spanwise wall-pressure correlation length estimated using Corcos model is found to be approximately 12 mm at 40 m/s and 5 mm at 16 m/s at stalling conditions. Far-field noise scales well with Strouhal number based on chord and U^5, indicating a compact dipolar scaling for separation and stall noise mechanisms.

I. Nomenclature

α_g	=	Geometric angle of attack (°)
c	=	Chord (m)
C_p	=	Mean wall-pressure coefficient
Δf	=	Frequency resolution (Hz)
γ^2	=	Spanwise coherence
Λ	=	Spanwise wall-pressure correlation length (m)
p_∞	=	Upstream pressure (Pa)
ϕ_{pp}	=	wall-pressure power spectral density (Pa^2/Hz)
ρ	=	density (Kg/m^3)
U_∞	=	upstream velocity (m/s)
z	=	distance between sensors (m)

II. Introduction

Aviation industry is one of the major contributors to noise, with the population living close to the airports affected most by the noise of airplanes taking-off and landing. To tackle this issue, the Federal Aviation Authority (FAA) [1] has imposed a maximum day-night average sound level of 65dB. In the approach conditions, the majority of the noise arises from the turbofan and the airframe [2]. Fan noise has been projected to increase with the advent of Ultra High By-pass Ratio (UHBR) engines [3, 4], and research is necessary to understand the mechanisms and reduce this noise source [5, 6]. Airframe noise arises mostly from the high-lift devices [7] and landing gears [8]. These high-lift devices operate under conditions where flow separation could be significant. The noise generation due to flow separation falls well inside the range of human hearing [9][10] and could be problematic. There have been many attempts at simulating and measuring the noise due to flow separation, to achieve complete understanding of the noise generation mechanisms involved. However, the complexity in simulating separated flow conditions lies in a high cost requirement, since the size and resolution in the spanwise direction necessary to resolve the spanwise length of the vortices (independent acoustic sources) responsible for noise generation [11] in separated flow regimes is higher than in an attached case. As was seen in the simulations of Christophe *et al.* [12] that were performed on a Controlled-Diffusion (CD) airfoil, a spanwise domain of 0.1 times chord which was enough to accurately resolve the structures in a attached boundary layer, failed to

*PhD candidate, Mechanical Engineering Department, sidharth.krishnan.kalyani@usherbrooke.ca.
†Professor, Mechanical Engineering Department, AIAA Lifetime Member, stephane.moreau@usherbrooke.ca.
‡Associate Professor, Aerodynamics, Wind Energy, Flight Performance and Propulsion Department, Member AIAA, d.ragni@tudelft.nl.

capture the statistically independent acoustic sources in flow condition with a higher adverse pressure gradient. Hence a prior knowledge of the spanwise lengthscale of vortices would be crucial in obtaining accurate results from simulations. On the other hand, experiments performed previously on airfoils under separation and stalling phenomena have not been able to compare with each other due to varying experimental conditions, such as different jet widths and test section configurations. A common observation from these experiments has shown that the low to mid-frequency generated noise is caused by the wall-pressure fluctuations induced by the vortices in the separated shear layer [9][13][14]. However, it was observed from the experiments of Moreau et al. [14] that the low frequency part of the noise was contaminated with the oscillation of the jet shear layers (which also fall under the low frequency category), which could mean an interaction of the jet shear layer with the vortices of the separated shear in a low jet width configuration (13 cm). This was seen as an increase in the low frequency amplitude, and can be easily misinterpreted as airfoil self-noise, but must instead be considered as a modification of background noise sources in the presence of the airfoil. This low frequency contamination, however was not observed in another configuration with a higher jet width (30 cm) in the same experiments of Moreau *et al.* [14], which also had different far-field noise characteristics. It was also previously observed by Moreau *et al.* [15] that the higher the jet width was, the earlier the onset of the laminar flow separation on the CD airfoil was, and the more forward the loading was. A different loading on the airfoil would lead to a different airfoil flow features, hence the results between different experiments with varying jet widths have not been directly comparable. Nevertheless, a complete flow mapping of the flow-field as the flow transitions from an attached to a completely detached one is still lacking in literature. For example, on the CD airfoil at low Reynolds number, transition occurs through a Laminar Separation bubble (LSB) that moves from the trailing region at geometric incidence $\alpha_g < 6°$ to the leading edge region (strong flow bifurcation) in a jet of 50 cm width. It has been observed that the size of the bubble grows from 4%-5% to 40% when the geometric incidence of the CD airfoil changes from $\alpha_g = 8°$ to $\alpha_g = 15°$. With increasing incidences, the bubble may or may not re-attach, an information which is not readily available. Hence the current investigation has the potential to address the above-mentioned gaps.

Based on the above considerations, the main goal of this paper is to understand the characteristics of flow-field, wall-pressure statistics and far-field noise of a CD airfoil, in an effort to address multiple objectives. They are,

- to understand the nature of wall-pressure and its relation to far-field noise statistics when the boundary layer transits from an attached to a completely detached one
- to analyse the effect of Reynolds number on the above mentioned statistics
- to explain differences in previous experimental results subject to similar experimental conditions [14][9]

A CD airfoil is to be utilized in the current study, which sees its application in many modern turbomachinery [16] and automotive blades [17].The boundary layer diffusion on the suction side of the CD airfoil is controlled by carefully designing the camber and thickness in such a way that from the highest point of velocity (at the leading edge) up until the trailing edge, the growth of boundary layer is kept as thin as possible. This also helps control the noise production, since noise produced by trailing edge scattering is proportional to the boundary layer thickness [18].

To this end, the paper is organized as follows. Section III introduces the experimental methodology, including the measurement configuration and techniques to be utilized in this study, and the proposed measurement campaign. Section IV discusses the results obtained in the present investigation.

III. Experimental methodology

The experiments were performed in the UdeS anechoic wind tunnel facility. The anechoic wind tunnel comprises of an anechoic room with a closed return type wind tunnel. The room dimensions are 7 x 5.5 x 4 m^3 (refer figure 1a). The nozzle outlet dimensions chosen for this campaign is 50 x 30 cm^2, since it was observed to have the a loading closest to the free stream conditions of the CD airfoil [15] [19]. The turbulence intensity in the jet is reported to be < 0.4% [20], due to a strong contraction ratio of 1:25. The CD airfoil to be used has a chord (c) of 0.1345 m and a span of 0.3 m and is vertically placed between two side plates, such that the jet width is 50 cm. The experiments are performed at two flow speeds, corresponding to 16 m/s and 40 m/s. This is done in an effort to understand the effect of Reynolds number on the separation and stalling phenomenon on the CD airfoil, and also compare with previous experimental results on a smaller jet width [20] of the UdeS wind tunnel.

Wall-pressure measurements were extracted using pinholes (0.5 mm diameter) already present on the CD profile (refer figure 1b). The capillary tube which extends out of the blade tip is connected to a block and branches out into two; one for measuring the steady pressure, where a capillary tube is extended by a long PVC soft tube to a differential pressure measurement sensor. The second part is connected to a Knowles FG 23329 P07 electret microphone, to measure the unsteady wall-pressures. The differential pressure measurement system (RCDB) used was manufactured by

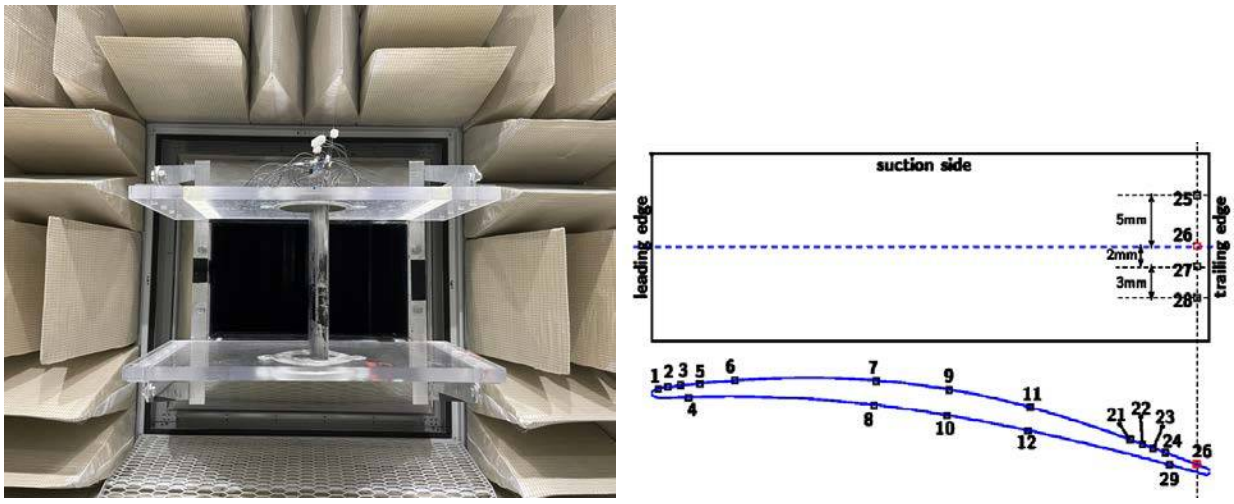

(a) **(b)**

Fig. 1 Experimental configuration at UdeS, a) the anechoic room with the nozzle exit and b) CD airfoil mock-up

Neal [21] for the purpose of measurement of differential pressure of a system of CD rotating blades. Far-field acoustic measurements were done using a PCB ICP sensor which was calibrated using a pistonphone. A NI module was utilized for acquiring the acoustics at a rate of 50 kHz for a period of 20 seconds.

IV. Results and discussion

From the experiments of Moreau *et al.* [14] at Ecole Centrale de Lyon (ECL), a lower relative jet width was observed to cause interaction of the separated vortices from the leading edge with the jet shear layer, modulating the low frequency content of the far-field noise. Relative jet width is defined as the ratio of jet width to the airfoil chord. This interaction was avoided with a high relative jet width (3.8) configuration. On comparison, the experiments performed at UdeS have similar relative jet width (3.71) as the high relative jet width case of ECL, and it is expected that there is limited or no interaction of the jet shear layer with the vortices of the separated shear layer.

A. *Flow-field analysis*

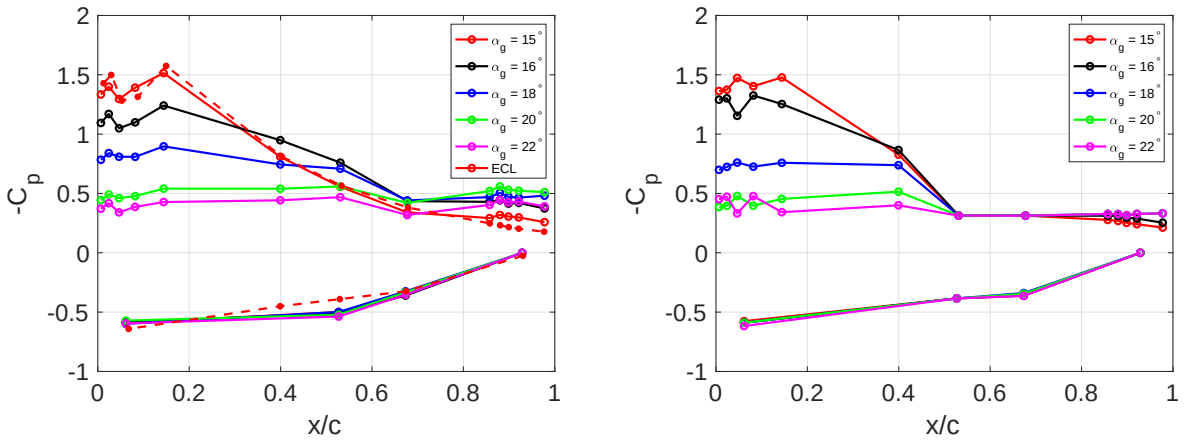

(a) **(b)**

Fig. 2 Mean wall-pressure coefficient C_p at, a) 16m/s and b) 40 m/s

From initial measurements, angles of attack chosen for the current investigation of the CD airfoil are α_g = 15°, 16°, 18°, 20°, 22°. In Fig. 2, the pressure coefficient C_p is shown on the CD airfoil surface as a function of dimensionless chord position with an origin at the leading edge. The pressure coefficient is defined as $C_p = (p - p_\infty)/(0.5\,\rho_\infty\,U_\infty^2)$, with p being the mean static pressure at each sensor location shown in Fig. 1b. p_∞, ρ_∞ and U_∞ are the upstream pressure, density and velocity measured at the nozzle exit respectively. At the leading edge, as mentioned earlier, the large hump corresponds to the large LSB that reattaches at 40% c [15, 22] for the case of α_g = 15° and a Turbulent Boundary Layer (TBL) is expected to convect past the Trailing-Edge (TE) of the airfoil. As shown in figure 2a, present measurements show a very similar trend when compared to the mean wall-pressure data extracted at ECL for the case of α_g = 15°. With increasing incidence, the airfoil is probably experiencing a soft stall. At α_g 16°-18°, the bubble is expected to be longer (the size of which increases with geometric incidence [23]) and the flow-field at the trailing edge is found to be similar between the two incidences, as will be shown later in the unsteady wall-pressure statistics. At α_g = 20 °, flow separation (LSB) has reached the trailing edge of the airfoil and the flow is completely separated from the airfoil. With further increase in incidence, the C_p falls further as the airfoil enters a deep-stall condition. Figure 2b shows the mean wall-pressure at a higher flow speed of 40 m/s. The bubble is expected to be shorter compared to the 16 m/s case [24]. Below α_g = 22 °, a small roll-off is clearly noticeable in the aft section of the airfoil as seen in the lower flow speed case of 15 ° and 16 °, which signals a local Adverse Pressure Gradient (APG). Hence the flat C_p could very much be indicating a Zero Pressure Gradient zone (ZPG) in the mid-chord region, or a partial flow separation with small vortices still rolling past the TE on the suction side. Finally, it can also be inferred that that deep stall is delayed with an increasing flow speed (or equivalenty increased Reynolds number based on the chord) on the CD airfoil.

B. ***Wall-pressure statistics***

The unsteady wall-pressure data obtained are converted from time to frequency domain using Welch's periodogram method [25], with a Hanning window size of 2^{12} and a 50% overlap, yielding a spectral resolution Δf of 12.5 Hz. Wall-pressure power spectral density ϕ_{pp} (PSD) thus obtained are compared at three different Remote Microphone Probe (RMP) locations, near the leading edge where the laminar boundary layer separates (RMP#6) in Fig. 3a , in the mid-chord location (RMP#11) in Fig. 3b, and near the trailing edge (RMP#25) in Fig. 3c. Sensors 6, 11 and 25 are chosen in each of these locations to analyse the variation in unsteady wall-pressure with angle of attack and Reynolds number. At all locations the levels slightly increase from 15 to 16° and then slightly drops at 18°. Increasing further the incidence to α_g = 20° and 22° seems to lead to a more significant reduction in overall wall-pressure spectra for both flow speeds, and even a faster roll-off at the leading edge. This could be possibly traced to a greater lift-off of the boundary layer near the leading edge. This drop also confirms that the airfoil is most likely stalled at these geometric incidences as shown in the distributions of mean pressure coefficient in Fig. 2. Overall, the slopes of the spectra do not seem to change with Reynolds number, but clearly there are more smaller structures and consequently a spectral roll-off at higher frequencies with an increase in Reynolds number based on the chord [26][15], a result which is common to all chordwise locations. At lower frequencies, the high speed case also shows flat spectra, whereas the low speed case is already decaying: yet, as shown below in the far-field noise spectra, the low frequency range can be contaminated by jet noise. In the mid-frequency range, a smooth transition from a -3 to -4 slope is observed in all spectra at both leading-edge and mid-chord locations, suggesting a separated flow (a -2 slope was found in strong APG regions of attached TBL in [15]). Only, at the trailing-edge sensor, the mid-frequency range shows a hump between 800 Hz and 3 kHz at all incidences for both Reynolds numbers (with a slight shift in frequency for 40 m/s). When compared to the attached TBL cases at α_g = 8° for both speeds, a very good agreement is found both in terms of shape and levels [11, 15, 22]. This hump around 1 kHz at 16 m/s was attributed to some vortex shedding mostly happening on the pressure side. This might be the same spurious noise mechanism that could be verified by some detailed velocity measurements in the near wake [21]. Actually, this was already verified in the previous LES at 15° (Fig. 14 in [12]). The decay at high frequencies for both flow speeds at all sensor locations is similar close to f^{-5}. This typical decay has been measured below several turbulent boundary layers (see all experimental ZPG data in [26] for instance), and attributed to the buffer layer. Finally, several spectra (particularly at all shown locations for the 22° case) exhibit a plateau beyond 4-6 kHz, which is quite similar to what was reported previously for the attached TBL cases at α_g = 8°: this could also be caused by the same wake noise source [27].

Spanwise wall-pressure coherence at the trailing edge for a spanwise distance (z) of 7 mm (between RMP#25 and RMP#27) is plotted in figures 4a and 4b for a Δf of 3.1 Hz. The spanwise coherence (γ^2) between two points on the

airfoil surface separated by Δz is defined as

$$\gamma^2(z, \Delta z, \omega) = \frac{|\phi_{pp}(z, \Delta z, \omega)|^2}{|\phi_{pp}(z, 0, \omega)|\,|\phi_{pp}(z + \Delta z, 0, \omega)|} \tag{1}$$

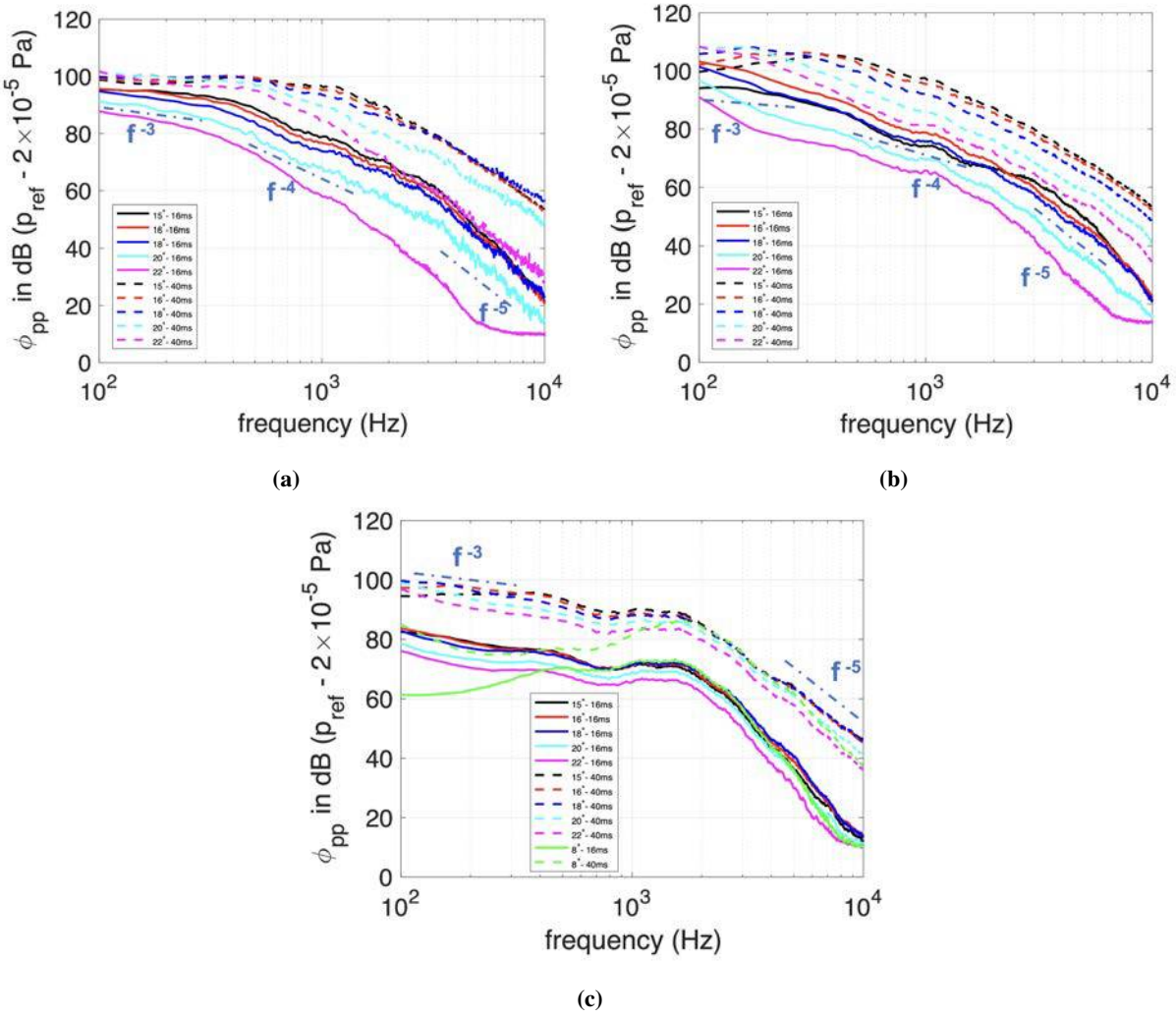

Fig. 3 Unsteady wall-pressures at three different sensors locations, a) RMP#6, b) RMP#11 and c) RMP#25

Clearly at these high angles of attack, large spanwise coherence levels are seen at low frequencies, below 200 Hz at 16 m/s and below 500 Hz at 40 m/s. Similarly to previous measurements on a NACA0012 airfoil, the coherence exhibit a bi-modal shape with a first peak at very low frequency (below 50 Hz) and a second one for several hundreds Hz. The global shift in frequencies with chord-based Reynolds number suggests that larger flow structures are involved at low speed as already suggested by the LSB size inferred from the mean pressure coefficient in Fig. 2a. Levels of coherence also increases with incidence and shifts towards lower frequencies for both flow speeds. This high correlation with distance is a characteristic of the increasing size of turbulent eddies with increasing incidence, as has been postulated in previous experiments [9, 13] and presently evidenced in Fig. 2. The two peaks yielding the bi-modal shape of the coherence have however different behaviors. Both grow with incidence, but the low frequency peak hardly move in frequency (slight shift to higher frequencies), whereas the second peak moves to lower frequencies. Both eventually merge at the highest studied angles-of-attack of 20° and 22° (deep stall). Similar variation is seen for both speeds suggesting that this is independent of the Reynolds number.

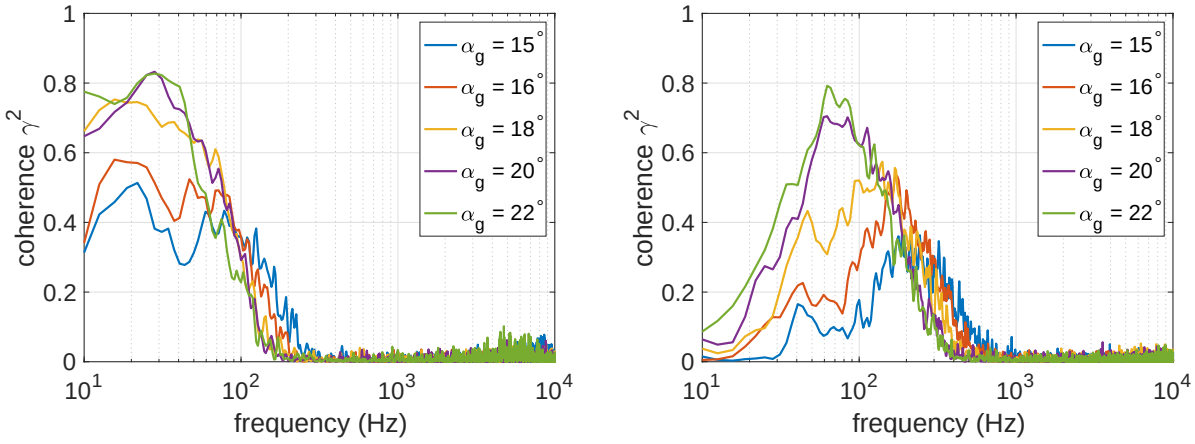

Fig. 4 Spanwise wall-pressure coherence between #RMP25 and #RMP27, a) at 16 m/s and b) at 40 m/s

The second hump is similar to what is observed at lower incidences for attached ZPG and APG TBL, and its decreasing part exhibit an exponential decay with frequency that can be fitted by a Corcos model [28]. Corcos found the streamwise and spanwise coherence to be well defined by an exponential function, with empirically determined coefficients representing the decay rate. The correlation in Eq. (1) then reads:

$$\gamma^2 = \exp\left(\frac{-4\pi z f}{b U_c}\right) \tag{2}$$

where b is the empirical constant and U_c is the convection velocity. The convection velocity has first been calculated in a three-step process. First, the data from RMP#24 and RMP#26 are bandpassed to retain the frequency range of interest. This data is then cross-correlated to find the time lag for maximum correlation as shown in Figs. 5a and 5b. Finally, the distance between RMP#24 and RMP#26 is divided by this time lag to obtain U_c. Mean U_c/U_∞ (U_∞ being

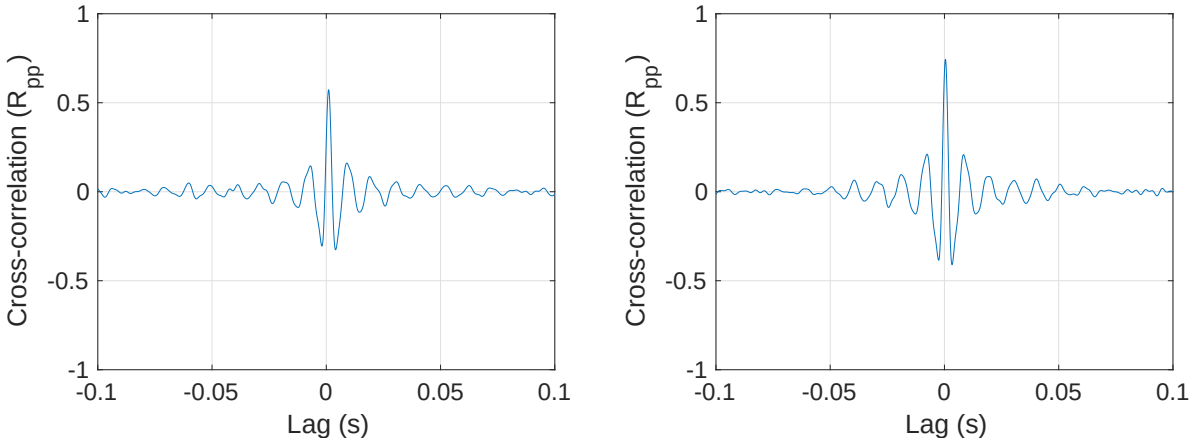

Fig. 5 Sample of convection velocity estimation using cross-correlation R_{pp} analysis of RMP#24 and RMP#26 in the frequency range of 100-300 Hz for a) 16 m/s and b) 40 m/s

the freestream velocity) thus calculated was estimated to be 0.52 for 16 m/s and 0.5 for 40 m/s, and this value agrees well with literature [29, 30] for strong APG flows. Based on the above estimates, the coherence data is fitted with the exponential function and is shown in Figs. 6a and 6b. $b = 0.4$ and $b = 0.42$ was found to give an appreciable fit to the coherence data for 40 m/s and 16 m/s, both as a function of frequency and spanwise distance.

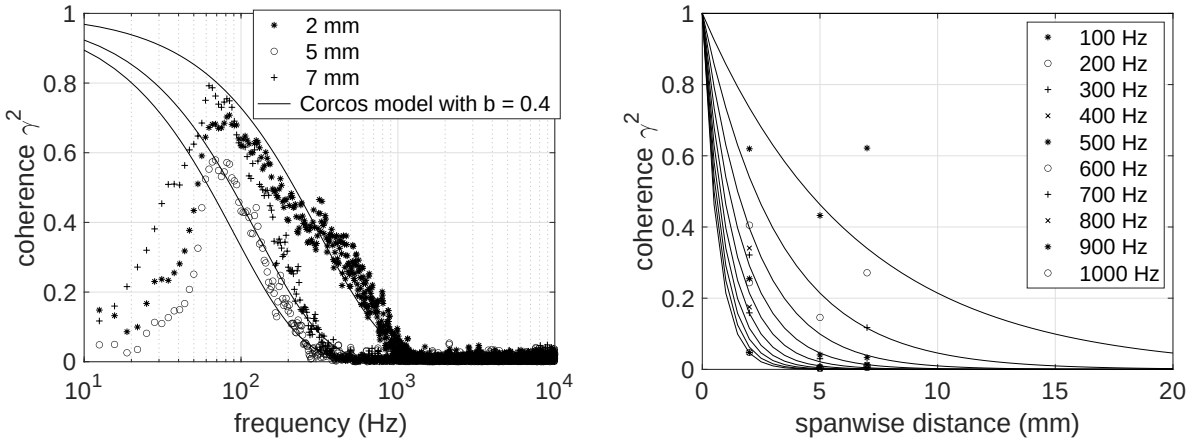

(a) **(b)**

Fig. 6 Corcos model for spanwise coherence at the TE at 40 m/s as a function of a) frequency and b) spanwise distance z

As a next step, spanwise pressure correlation length (Λ) has been calculated by integrating the exponential function along the spanwise direction (figure 6b) [31] as

$$\Lambda(f) = \int_0^\infty \exp\left(\frac{-2\pi z f}{bU_c}\right) dz$$

and is shown in figure 7a. From this analysis, the largest spanwise pressure correlation length scale for the CD airfoil at stalling angles of attack was extracted to be 0.09c and 0.04c for 40 m/s and 16 m/s respectively.

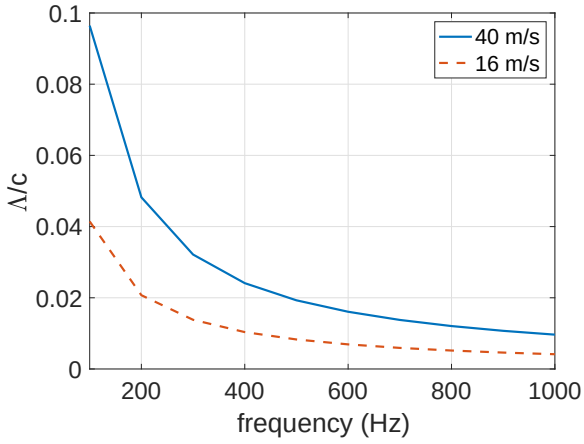

(a)

Fig. 7 Normalised spanwise wall-pressure correlation length (Λ/c)

C. *Far-field acoustics*

Before getting into the far-field noise spectra, some correlation between unsteady wall-pressures and far-field noise (shown in the Figs. 8a and 8b) is first studied. Assuming that the trailing edge causes diffraction of eddies and is mainly responsible for the far-field acoustics (the wall-pressure spectra already suggest other noise sources), coherence between the trailing edge sensor and the far-field microphone has been analysed. There is only significant correlation over the

same frequency range as observed previously in the spanwise coherence of wall-pressure fluctuations. Similar bi-modal shape is found. Yet, the behaviors of the peaks are different. On the one hand, only the levels of the low-frequency one increase with incidence, with a shift to increasing frequencies clearly evidenced this time. On the other hand, the second peak has no longer a monotonic behavior, but with a similar shift to lower frequencies as the spanwise coherence of wall-pressure fluctuations. Indeed, its levels first grow to similar levels of 0.4 for both incidences of 16° and 18° (onset of stall), and then sharply decreases for 20° and 22° (deep stall). For the latter it has almost disappeared. At high frequencies, for both speeds and all incidences, no significant correlations is obtained as previously found at the lowest angles of attack (8° for instance).

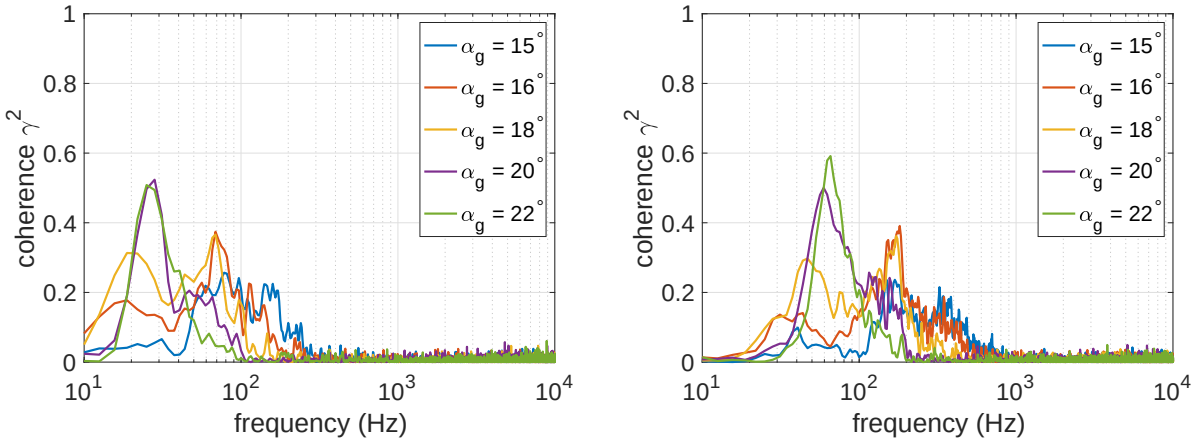

Fig. 8 Correlation between #RMP26 and far-field suction side microphone at, a) 16 m/s and b) 40 m/s

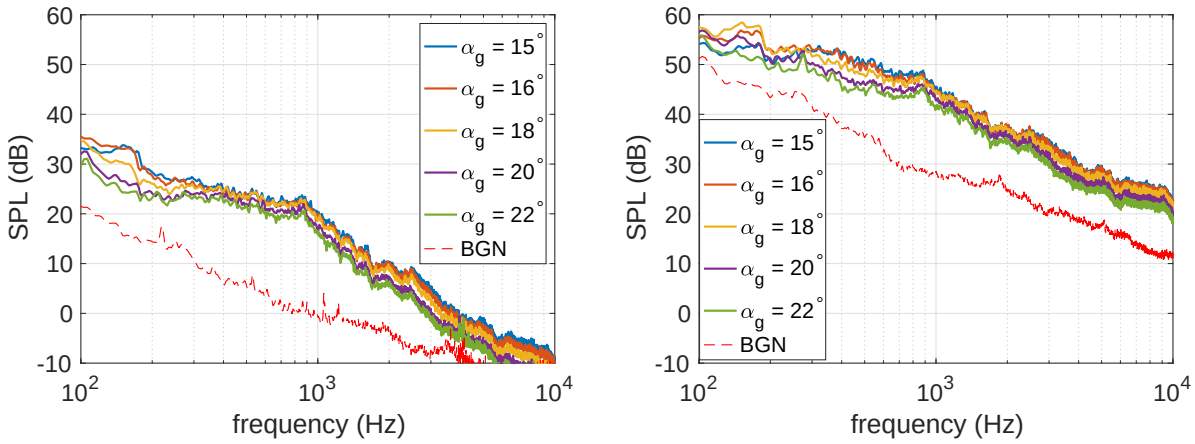

Fig. 9 Far-field acoustic pressure at various geometric incidences and for flow speed: a) 16 m/s and b) 40 m/s

Far-field noise spectra have been plotted for both flow speeds along with the background noise in Figs. 9a and 9b. The background noise is lower by around 10 dB compared to the airfoil self-noise in the range compared, which shows the capability of the wind tunnel for such a study. For both flow speeds, the noise levels decrease with increasing geometric incidence. The spectra at 16 m/s is similar to the results obtained by Lacagnina *et al.* [9] and has an overall broadband nature. At 40 m/s, small peaks (black arrow) are noticeable centered at 275 Hz for stall and post stall cases. During this investigation, the intensity of these peaks were seen to increase with increasing flow speeds.

Finally, scaling laws were extracted for the two flow velocities and is shown in Fig. 10 [14]. When the PSD is

normalized by U^5, a good collapse is observed except at very low Strouhal numbers, indicating a dominant compact dipolar nature of separation and stalling noise [32]. All these results indicate that the CD airfoil undergoes a soft stall in the open jet configuration of UdeS and is a good mock-up to study the separation and stalling aeroacoustics. It is also worthwhile to mention that comparisons of these results were also done with the previous measurements [15] on the CD airfoil at 15°, which showed a good agreement.

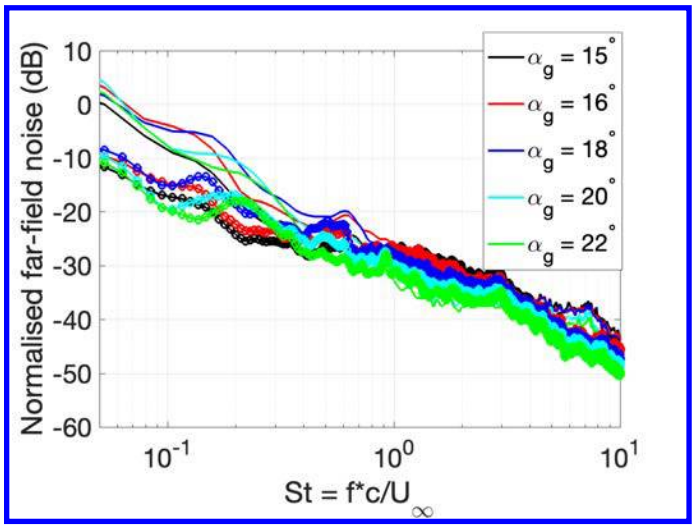

Fig. 10 Comparison of far-field noise spectra normalized by U^5 as a function of Strouhal based on chord (c) of the airfoil (Solid lines - 16 m/s and dotted lines - 40 m/s)

V. Conclusions and outlook

A flow-field and noise characterization of the CD airfoil was performed in the UdeS anechoic wind tunnel at high geometric angles of attack from $\alpha_g = 15°$ to $\alpha_g = 22°$, for two different speeds of 16 m/s and 40 m/s to study the effect of Reynolds numbers. First mean wall-pressure measurements have been achieved to characterize the airfoil loading in the present large 50 cm jet width. Secondly, simultaneous near-field wall pressure statistics and far-field acoustic have been collected to determine both the noise sources and the sound generated in these various flow conditions.

Results obtained from wall-pressures and far-field noise have been favorably compared with previous experiments at $\alpha_g = 15°$ conducted in the ECL anechoic wind tunnel with the same jet width. The large LSB that covers 40% of the chord is observed and the same larger low-frequency fluctuation content is found. The 16° and 18° cases show an increase of the LSB, which covers the entire chord in the latter case signalling the beginning of stall. At 20° stall characterized by a flat pressure distribution on the suction side is reached. The levels drop even further at 22° sign of deep stall. As for the effect of Reynolds number, stalling seems to be delayed on the 40 m/s case, where $\alpha_g = 22°$ could represent a condition where the airfoil just enters stall, unlike the deep stall case at the same incidence at 16 m/s.

Wall-pressure spectral comparison at the TE region reveals that there could be a possibility of small vortical structures convecting over the TE, even when the airfoil is stalled, which has been verified from positive values of convection velocity at the TE. The spanwise coherence results show that coherence shifts towards low frequencies with increasing incidence, and an overall shift to higher frequencies is noticed with an increase in flow speed. A Corcos model fit to the coherence data provides an estimate for Λ to be 12 mm at 40 m/s and 5 mm at 16 m/s for the CD airfoil at $\alpha_g = 22°$. The far-field noise levels grow up to 16° and then decrease beyond 18° confirming the onset of stall. Tonal signature is evidenced for stalling geometric incidences at 40 m/s around 275 Hz, and it has been seen to increase in intensity with increasing flow speed. A good collapse is observed when scaling the far-field noise spectra with U^5 and Strouhal number based on chord, indicating a compact dipolar nature of separation and stalling noise. Planar PIV and Hot-wire measurements simultaneously with the wall-pressure and far-field will be performed in the near future to validate the findings of this experiment.

References

[1] Finegold, L. S., Finegold, M. S., and Maling Jr, G. C., "An overview of US noise policy," *Noise Control Engineering Journal*, Vol. 51, No. 3, 2003, pp. 131–142.

[2] Peake, N., and Parry, A. B., "Modern challenges facing turbomachinery aeroacoustics," *Annual Review of Fluid Mechanics*, Vol. 44, 2012, pp. 227–248.

[3] Moreau, S., "Turbomachinery Noise Predictions: Present and Future," *Acoustics*, Vol. 1, 2019, pp. 92–116. https://doi.org/10.3813/AAA.918372.

[4] Moreau, S., *A review of turbomachinery noise: from analytical models to high-fidelity simulations*, Vol. Fundamentals of High Lift for Future Civil Aircraft, Springer Nature Switzerland AG, 2020. https://doi.org/10.3813/AAA.918372.

[5] Arroyo, C. P., Kholodov, P., Sanjosé, M., and Moreau, S., "CFD modeling of a realistic turbofan blade for noise prediction. Part 1: Aerodynamics," *Proceedings of the Global Power and Propulsion Society (GPPS, 2019)*, 2019.

[6] Koch, R., Sanjose, M., and Moreau, S., "Numerical investigation of noise sources in a single airfoil tip-leakage flow," *25th AIAA/CEAS Aeroacoustics Conference*, 2019, p. 2625.

[7] Perennes, S., and Roger, M., "Aerodynamic noise of a two-dimensional wing with high-lift devices," *4th AIAA/CEAS aeroacoustics conference*, Toulouse,France, 1998, p. 2338.

[8] Manoha, E., Bulté, J., and Caruelle, B., "LAGOON: an experimental database for the validation of CFD/CAA methods for landing gear noise prediction," *14th AIAA/CEAS aeroacoustics conference (29th AIAA aeroacoustics conference)*, Vancouver, British Columbia, Canada, 2008, p. 2816.

[9] Lacagnina, G., Chaitanya, P., Berk, T., Kim, J., Joseph, P., Ganapathisubramani, B., Hasheminejad, S., Chong, T., Stalnov, O., Choi, K., et al., "Investigation on the mechanism for the aerofoil noise near stall conditions," *Physical Review Fluids*, 2019.

[10] Paterson, R. W., Amiet, R. K., and Munch, C. L., "Isolated airfoil-tip vortex interaction noise," *Journal of Aircraft*, Vol. 12, No. 1, 1975, pp. 34–40.

[11] Christophe, J., and Moreau, S., "LES of the trailing-edge flow and noise of a controlled-diffusion airfoil at high angle of attack," *Proceedings of the Summer Program*, Stanford, California, U.S.A, 2008, p. 305.

[12] Christophe, J., Anthoine, J., and Moreau, S., "Trailing edge noise of a controlled-diffusion airfoil at moderate and high angle of attack," *15th AIAA/CEAS Aeroacoustics Conference (30th AIAA Aeroacoustics Conference)*, Miami, Florida, 2009, p. 3196.

[13] Mayer, Y., Zang, B., and Azarpeyvand, M., "Aeroacoustic characteristics of a NACA 0012 airfoil for attached and stalled flow conditions," *25th AIAA/CEAS Aeroacoustics Conference*, Delft, The Netherlands, 2019, p. 2530.

[14] Moreau, S., Roger, M., and Christophe, J., "Flow features and self-noise of airfoils near stall or in stall," *15th AIAA/CEAS Aeroacoustics Conference (30th AIAA Aeroacoustics Conference)*, Miami, Florida, 2009, p. 3198.

[15] Moreau, S., and Roger, M., "Effect of airfoil aerodynamic loading on trailing edge noise sources," *AIAA journal*, Vol. 43, No. 1, 2005, pp. 41–52.

[16] Kholodov, P., and Moreau, S., "Identification of noise sources in a realistic turbofan rotor using Large Eddy Simulation," *Acoustics*, Vol. 2, Multidisciplinary Digital Publishing Institute, 2020, pp. 691–706.

[17] Caro, S., and Moreau, S., "Aeroacoustic modelling of low pressure axial flow fans," *6th Aeroacoustics Conference and Exhibit*, Lahaina,HI,U.S.A., 2000, p. 2094.

[18] Brooks, T. F., and Hodgson, T. H., "Trailing edge noise prediction from measured surface pressures," *Journal of sound and vibration*, Vol. 78, No. 1, 1981, pp. 69–117.

[19] Moreau, S., Henner, M., Iaccarino, G., Wang, M., and Roger, M., "Analysis of flow conditions in freejet experiments for studying airfoil self-noise," *AIAA journal*, Vol. 41, No. 10, 2003, pp. 1895–1905.

[20] Padois, T., Laffay, P., Idier, A., and Moreau, S., "Detailed experimental investigation of the aeroacoustic field around a Controlled-Diffusion airfoil," *21st AIAA/CEAS aeroacoustics conference*, Dallas, TX, U.S.A., 2015, p. 2205.

[21] Neal, D. R., "The effects of rotation on the flow field over a controlled-diffusion airfoil," Ph.D. thesis, Michigan State University, 2010.

[22] Wu, H., Sanjose, M., Moreau, S., and Sandberg, R. D., "Direct numerical simulation of the self-noise radiated by the installed Controlled-Diffusion airfoil at transitional Reynolds number," *2018 AIAA/CEAS Aeroacoustics Conference*, Atlanta, Georgia, 2018, p. 3797.

[23] O'meara, M., and Mueller, T. J., "Laminar separation bubble characteristics on an airfoil at low Reynolds numbers," *AIAA journal*, Vol. 25, No. 8, 1987, pp. 1033–1041.

[24] Lin, J. M., and Pauley, L. L., "Low-Reynolds-number separation on an airfoil," *AIAA journal*, Vol. 34, No. 8, 1996, pp. 1570–1577.

[25] Welch, P., "The use of fast Fourier transform for the estimation of power spectra: a method based on time averaging over short, modified periodograms," *IEEE Transactions on audio and electroacoustics*, Vol. 15, No. 2, 1967, pp. 70–73.

[26] Goody, M., "Empirical spectral model of surface pressure fluctuations," *AIAA journal*, Vol. 42, No. 9, 2004, pp. 1788–1794.

[27] Wu, H., Moreau, S., and Sandberg, R. D., "On the noise generated by a controlled-diffusion aerofoil at Rec= 1.5× 105," *Journal of Sound and Vibration*, Vol. 487, 2020, p. 115620.

[28] Corcos, G., "The structure of the turbulent pressure field in boundary-layer flows," *Journal of Fluid Mechanics*, Vol. 18, No. 3, 1964, pp. 353–378.

[29] Na, Y., and Moin, P., "The structure of wall-pressure fluctuations in turbulent boundary layers with adverse pressure gradient and separation," *Journal of Fluid Mechanics*, Vol. 377, 1998, pp. 347–373.

[30] Schloemer, H. H., "Effects of Pressure Gradients on Turbulent-Boundary-Layer Wall-Pressure Fluctuations," *The journal of the acoustical society of America*, Vol. 42, No. 1, 1967, pp. 93–113.

[31] Hu, N., "Coherence of wall pressure fluctuations in zero and adverse pressure gradients," *Journal of Sound and Vibration*, Vol. 511, 2021, p. 116316.

[32] Glegg, S., and Devenport, W., *Aeroacoustics of low mach number flows: fundamentals, analysis, AND measurement*, Academic Press, 2017.